Pet. Sci. (2017) 14:605–615
DOI 10.1007/s12182-017-0178-x

ORIGINAL PAPER

Efficient ozonation of reverse osmosis concentrates from petroleum refinery wastewater using composite metal oxide-loaded alumina

Yu Chen[1] · Chun-Mao Chen[1] · Brandon A. Yoza[2] · Qing X. Li[3] · Shao-Hui Guo[1] · Ping Wang[1] · Shi-Jie Dong[1] · Qing-Hong Wang[1]

Received: 15 December 2016 / Published online: 13 July 2017

Abstract Novel Mn–Fe–Mg- and Mn–Fe–Ce-loaded alumina (Mn–Fe–Mg/Al_2O_3 and Mn–Fe–Ce/Al_2O_3) were developed to catalytically ozonate reverse osmosis concentrates generated from petroleum refinery wastewaters (PRW-ROC). Highly dispersed 100–300-nm deposits of composite multivalent metal oxides of Mn (Mn^{2+}, Mn^{3+}, and Mn^{4+}), Fe (Fe^{2+} and Fe^{3+}) and Mg (Mg^{2+}), or Ce (Ce^{4+}) were achieved on Al_2O_3 supports. The developed Mn–Fe–Mg/Al_2O_3 and Mn–Fe–Ce/Al_2O_3 exhibited higher catalytic activity during the ozonation of PRW-ROC than Mn–Fe/Al_2O_3, Mn/Al_2O_3, Fe/Al_2O_3, and Al_2O_3. Chemical oxygen demand removal by Mn–Fe–Mg/Al_2O_3- or Mn–Fe–Ce/Al_2O_3-catalyzed ozonation increased by 23.9% and 23.2%, respectively, in comparison with single ozonation. Mn–Fe–Mg/Al_2O_3 and Mn–Fe–Ce/Al_2O_3 notably promoted ·OH generation and ·OH-mediated oxidation. This study demonstrated the potential use of composite metal oxide-loaded Al_2O_3 in advanced treatment of bio-recalcitrant wastewaters.

Keywords Petroleum refinery wastewater · Reverse osmosis concentrate · Catalytic ozonation · Composite metal oxide

1 Introduction

The need for freshwater and its conservation are motivating factors for treatment of wastewaters generated by petroleum refining industries. Reverse osmosis (RO) systems are widely used during the treatment and reclamation processes for the effluent from petroleum refinery wastewater (PRW) plants (Pérez-González et al. 2012). In China, 70 wt%–80 wt% of the effluent is reclaimed using RO systems and used as the high-quality feed water for steam production. The remaining 20 wt%–30 wt% of RO concentrate (ROC) contains petroleum-derived chemicals (Chen et al. 2016). Direct discharge of the ROC threatens the ecological environment and human health. The organics in ROC generated from PRW reclamation (PRW-ROC) need to be reduced to eliminate these negative impacts and to meet increasingly stringent discharge standards (Moreira et al. 2017). Previous work has already investigated the use of physicochemical and biological treatments; however, low concentrations and biologically recalcitrant organic matter suggest these methods are unsuitable (Bagastyo et al. 2013).

Advanced oxidation processes (AOPs) are the preferred advanced treatment method during reclamation of various municipal and industrial wastewater ROC products (Joo and Tansel 2015; Ren et al. 2016). These methods, including ozonation (Dialynas et al. 2008), Fenton oxidation (Zhou et al. 2012), photocatalysis (Joo and Tansel 2015), photooxidation (Umar et al. 2016), sonolysis (Pérez-González et al. 2012), or electrochemical oxidation

Yu Chen and Chun-Mao Chen have contributed equally to this work.

✉ Qing-Hong Wang
wangqhqh@163.com

[1] State Key Laboratory of Petroleum Pollution Control, Beijing Key Laboratory of Oil and Gas Pollution Control, China University of Petroleum, Beijing 102249, China

[2] Hawaii Natural Energy Institute, University of Hawaii at Manoa, Honolulu, HI 96822, USA

[3] Department of Molecular Biosciences and Bioengineering, University of Hawaii at Manoa, Honolulu, HI 96822, USA

Edited by Xiu-Qin Zhu

(Bagastyo et al. 2011; Van Hege et al. 2002), can provide efficient removal of low concentration and recalcitrant organics. Among these, the heterogeneous catalytic ozonation processes (COPs) are the most promising, as they are economical, highly efficient, and simple in their application. The predominant role of catalysts for heterogeneous COP treatment is decomposing ozone into more active species such as hydroxyl radicals (·OH), and/or for the adsorption of specific organics that can react with dissolved ozone (Chen et al. 2015). A wide variety of catalysts have been developed for COPs; however, most synthesized or prepared catalysts are costly, limiting their industrial application.

Alumina (Al_2O_3) and metal oxide-loaded Al_2O_3 have been widely applied in COPs. These materials have highly active and large surface area, good mechanical properties and are stable (Einaga and Futamura 2005; Pocostales et al. 2011; Keykavoos et al. 2013; Vittenet et al. 2015). Industrial grade γ-Al_2O_3 particles have been used for enhanced ozonation of petrochemical effluents (Vittenet et al. 2015). Ti/Al_2O_3 (Bing et al. 2017), Ru/Al_2O_3 (Zhou et al. 2007), and V/Al_2O_3 (Qi et al. 2009) are efficient catalysts for the treatment of recalcitrant organics such as dimethyl phthalate and 1, 2-dichlorobenzene. Mn/Al_2O_3 is another powerful catalyst for removal of bio-recalcitrant organics. Mn/Al_2O_3 can significantly produce ·OH when it reacts with ozone, resulting in enhanced catalytic degradation of atrazine (Rosal et al. 2010a), and fenofibric acid (Rosal et al. 2010b). Fe/Al_2O_3 exhibited both significant inhibition of BrO_3^- formation and high total organic carbon removal for a Br-containing raw water (Nie et al. 2014). Numerous studies have revealed that composite metal oxides loaded on Al_2O_3 supports exhibited high catalytic activity compared with single metal oxide loading (Tong et al. 2010). Mn–Fe–Cu/Al_2O_3 enhanced catalytic ozonation of PRW compared with single or double metal oxide-loaded Al_2O_3, a result from interactions between the composite metal oxides on the Al_2O_3 surface (Chen et al. 2015). Magnesium oxides, that include MgO nanocrystals and MgO/granular activated carbon (GAC), have potential for ozonation of bio-recalcitrant organics including phenols (Moussavi et al. 2014), benzene homologues (Rezaei et al. 2016), and dye pollutants (Moussavi and Mahmoudi 2009). During the ozonation of catechol that is catalyzed by MgO/GAC, ·OH was responsible for its degradation and mineralization, and this reaction rate constant was six times greater than single ozonation (Moussavi et al. 2014). Catalysts containing Ce have also been studied for the ozonation of *p*-chlorobenzoic acid (Bing et al. 2013), bezafibrate (Xu et al. 2016), dimethyl phthalate (Yan et al. 2013), and tonalide (Santiago-Morales et al. 2012). However, their applicability for wastewater treatment has not yet been reported.

In this study, novel composite metal oxide-loaded Al_2O_3 catalysts, including Mn–Fe–Mg/Al_2O_3 and Mn–Fe–Ce/Al_2O_3, were prepared and characterized. The potential use of these catalysts for the advanced treatment of PRW-ROC using COP was investigated. Insights into these catalytic mechanisms are also provided.

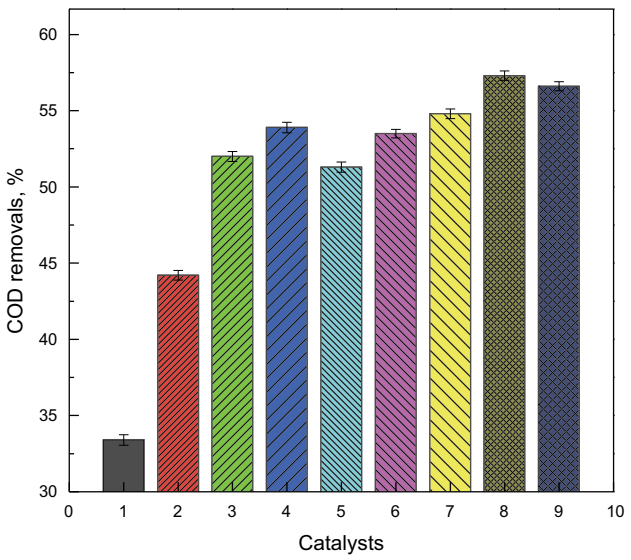

Fig. 1 COD removals for PRW-ROC using single ozonation and various COPs (0.5 g catalyst, 5 mg/min ozone, 30 °C, and 40 min). *1* single ozonation, *2* Al_2O_3-COP, *3* Fe/Al_2O_3-COP, *4* Fe/Al_2O_3(s)-COP, *5* Mn/Al_2O_3-COP, *6* Mn/Al_2O_3(s)-COP, *7* Mn–Fe/Al_2O_3-COP, *8* Mn–Fe–Mg/Al_2O_3-COP, and *9* Mn–Fe-Ce/Al_2O_3-COP

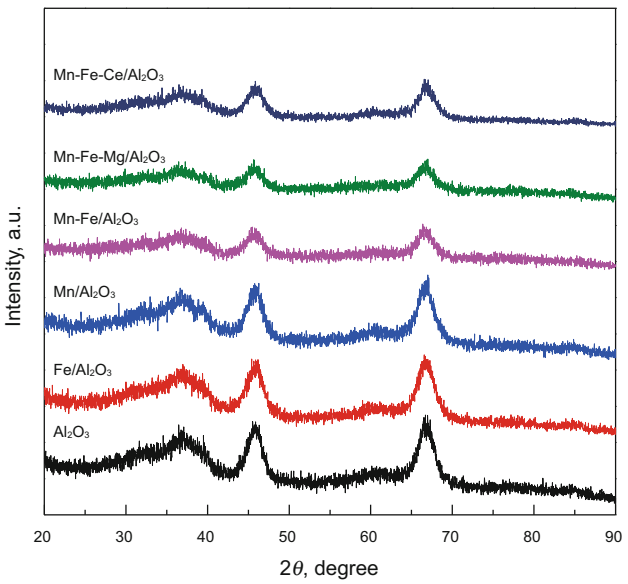

Fig. 2 XRD patterns of Al_2O_3 and metal oxide-loaded Al_2O_3 catalysts

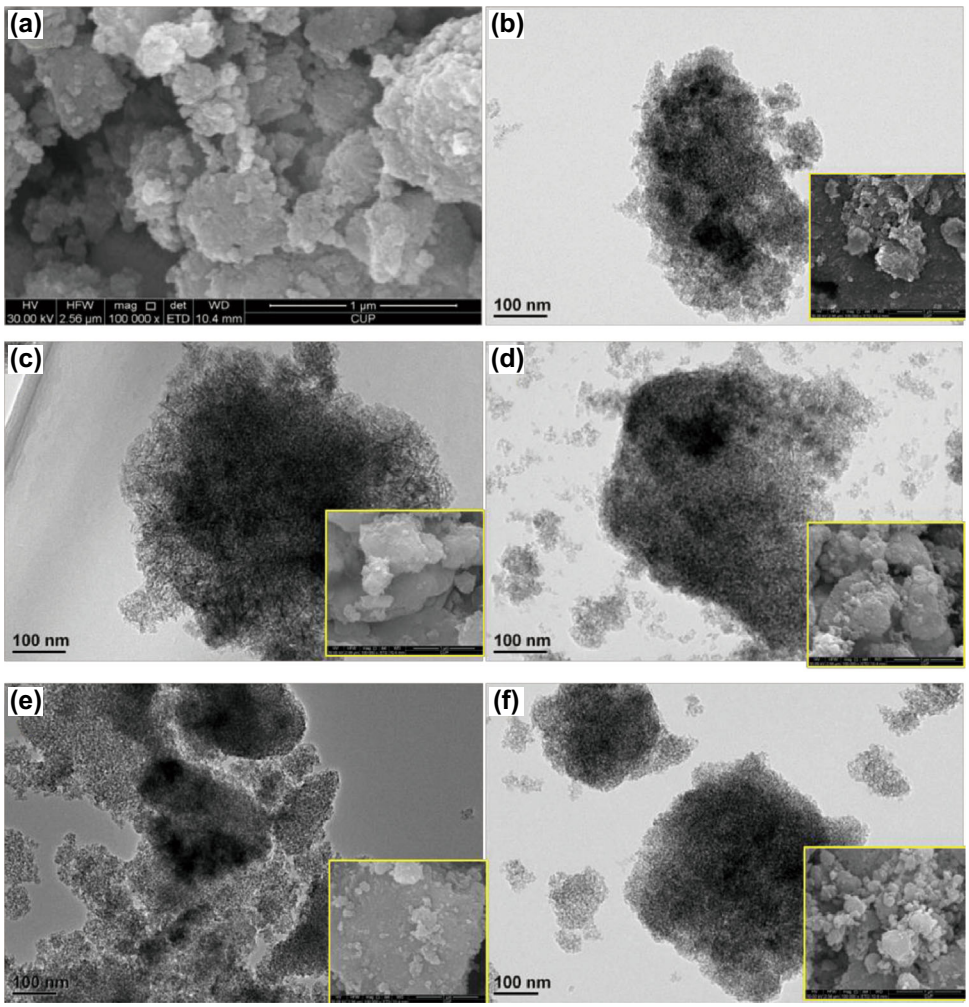

Fig. 3 SEM micrographs of Al_2O_3 (**a**), and SEM–TEM micrographs of Fe/Al_2O_3 (**b**), Mn/Al_2O_3 (**c**), $Mn–Fe/Al_2O_3$ (**d**), $Mn–Fe–Mg/Al_2O_3$ (**e**), and $Mn–Fe–Ce/Al_2O_3$ (**f**) catalysts

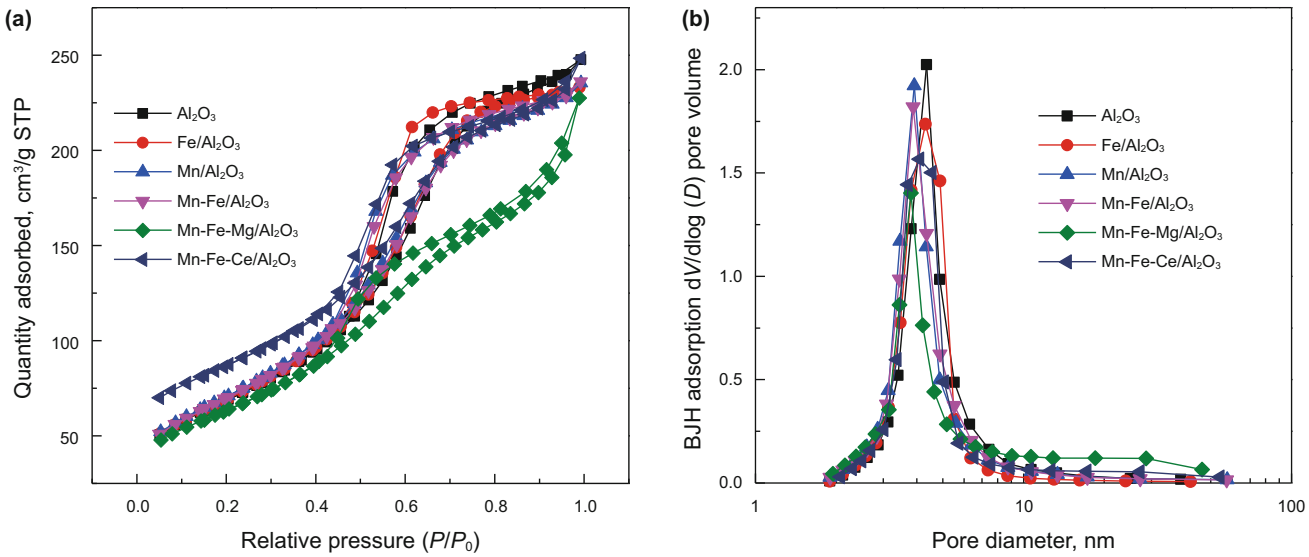

Fig. 4 Isotherms (**a**) and pore distribution curves (**b**) of Al_2O_3 and metal oxide-loaded Al_2O_3 catalysts by N_2 adsorption–desorption

Table 1 Surface areas and pore structures of Al_2O_3 and metal oxide-loaded Al_2O_3 catalysts

Catalysts	S_{BET}, m^2/g	V_P, cm^3/g	D_a, nm
Al_2O_3	250	0.38	6.1
Fe/Al_2O_3	252	0.36	5.7
Mn/Al_2O_3	258	0.36	5.6
$Mn–Fe/Al_2O_3$	255	0.37	5.7
$Mn–Fe–Mg/Al_2O_3$	230	0.35	6.1
$Mn–Fe–Ce/Al_2O_3$	242	0.35	5.8

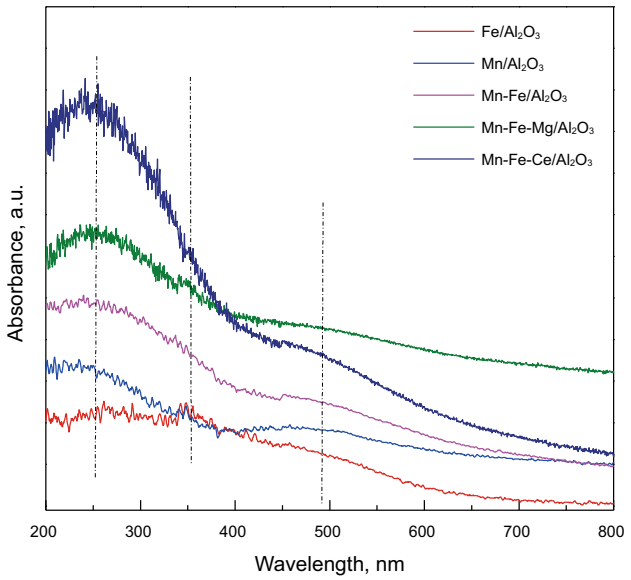

Fig. 5 UV-Vis patterns of metal oxide-loaded catalysts

2 Experimental

2.1 Preparation of catalysts

Commercial pseudoboehemite (65.6 wt% of Al_2O_3) was purchased from Chalco Shandong Co., Ltd. (China). $Fe(NO_3)_3·9H_2O$ (≥98.5 wt%), $Mn(NO_3)_2·4H_2O$ solution (50 wt%), $Mg(NO_3)_2·6H_2O$ (≥99.0 wt%), and $Ce(NO_3)_3·6H_2O$ (≥99.0 wt%) were obtained from Beijing Chemical Reagents Co., China. The catalysts were prepared according to the incipient wetness impregnation method. 60.0 g boehmite was impregnated with the mixture solution of 4.57 g $Mn(NO_3)_2·4H_2O$, 4.57 g $Fe(NO_3)_3·9H_2O$ and 0.79 g $Mg(NO_3)_2·6H_2O$, or 0.35 g $Ce(NO_3)_3·6H_2O$ (≥99.0 wt%) to yield Mn–Fe–Mg/Al_2O_3 or Mn–Fe–Ce/Al_2O_3 catalysts.

Impregnation of 60.0 g boehmite with a mixture solution of 4.55 g $Mn(NO_3)_2·4H_2O$ and 4.56 g $Fe(NO_3)_3·9H_2O$ yielded Mn–Fe/Al_2O_3 catalyst. Impregnation of 60.0 g boehmite with 4.45 or 9.00 g $Mn(NO_3)_2·4H_2O$ yielded Mn/Al_2O_3 or Mn/Al_2O_3 (s) catalysts, respectively. Impregnation of 60.0 g boehmite with 4.46 or 9.00 g $Fe(NO_3)_3·9H_2O$ yielded Fe/Al_2O_3 or Fe/Al_2O_3 (s) catalysts, respectively. The impregnated samples were calcined at 550 °C for 4 h in air after drying at 120 °C for 12 h. Al_2O_3 was prepared from pseudoboehemite by calcination at 550 °C for 4 h in air.

2.2 Characterization of catalysts

The crystal forms were observed by X-ray powder diffraction (XRD) using a D8 advance X-ray powder diffractometer (Bruker, Germany) with 40.0 kV working voltage and 40.0 mA current and a copper target X-ray tube. The specific surface area and pore size distribution were determined using a Tristar II 3020 surface area and porosity analyzer (Micromeritics, USA) with liquid nitrogen cooling at −196 °C. The total surface areas (S_{BET}) and total pore volume (V_p) were calculated according to Brunauer–Emmett–Teller (BET) and Barrett–Joyner–Halenda (BJH) methods, respectively. The bulk chemical composition was determined by X-ray fluorescence (XRF) analysis with an AX XRF analyzer (Axiosm, Netherlands). The elemental surface distribution was determined by X-ray photoelectron spectroscopy (XPS) analysis with a PHI Quantera SXM X-ray photoelectron spectrometer (ULVAC, USA), where all measured values of the binding energy (BE) were referred to the C_{1S} line at 284.8 eV. The diffuse reflectance spectra were recorded on a U-4100 UV–Vis spectrophotometer (Hitachi, Japan). The surface morphology was observed with a Tecnai G2 F20 transmission electron microscope (TEM) and a Quanta 200F scanning electron microscope (SEM) (FEI, USA). The point of zero charge (pH_{pzc}) was determined according to the pH drift method (Altenor et al. 2009).

2.3 Ozonation of PRW-ROC

The PRW-ROC used was collected directly from the RO unit of a wastewater treatment plant in Liaohe Petrochemical Co., China National Petroleum Corp. The ranges of pH values, 5-day biochemical oxygen demand (BOD_5), chemical oxygen demand (COD), and electric conductivity (25 °C) were determined. These were 8.0 to 8.5, 9.2 to 16.3, 105.6 to 125.3 mg/L, and 4438 to 5130 μS/cm, respectively. The COD concentration of PRW-ROC failed to meet the current Emission Standard of Pollutants for Petroleum Refining Industry of China (GB 31570-2015) in which the allowable COD concentration is lower than 60 mg/L. The BOD_5/COD ratios of PRW-ROC were ranged from 0.09 to 0.13. Due to low biodegradability, COP was determined as an efficient advanced treatment method for PRW-ROC.

The experimental system was constructed with an oxygen tank, RQ-02 ozone generator (Ruiqing, China), 200-mL quartz column reactor, flow meter, and an exhaust

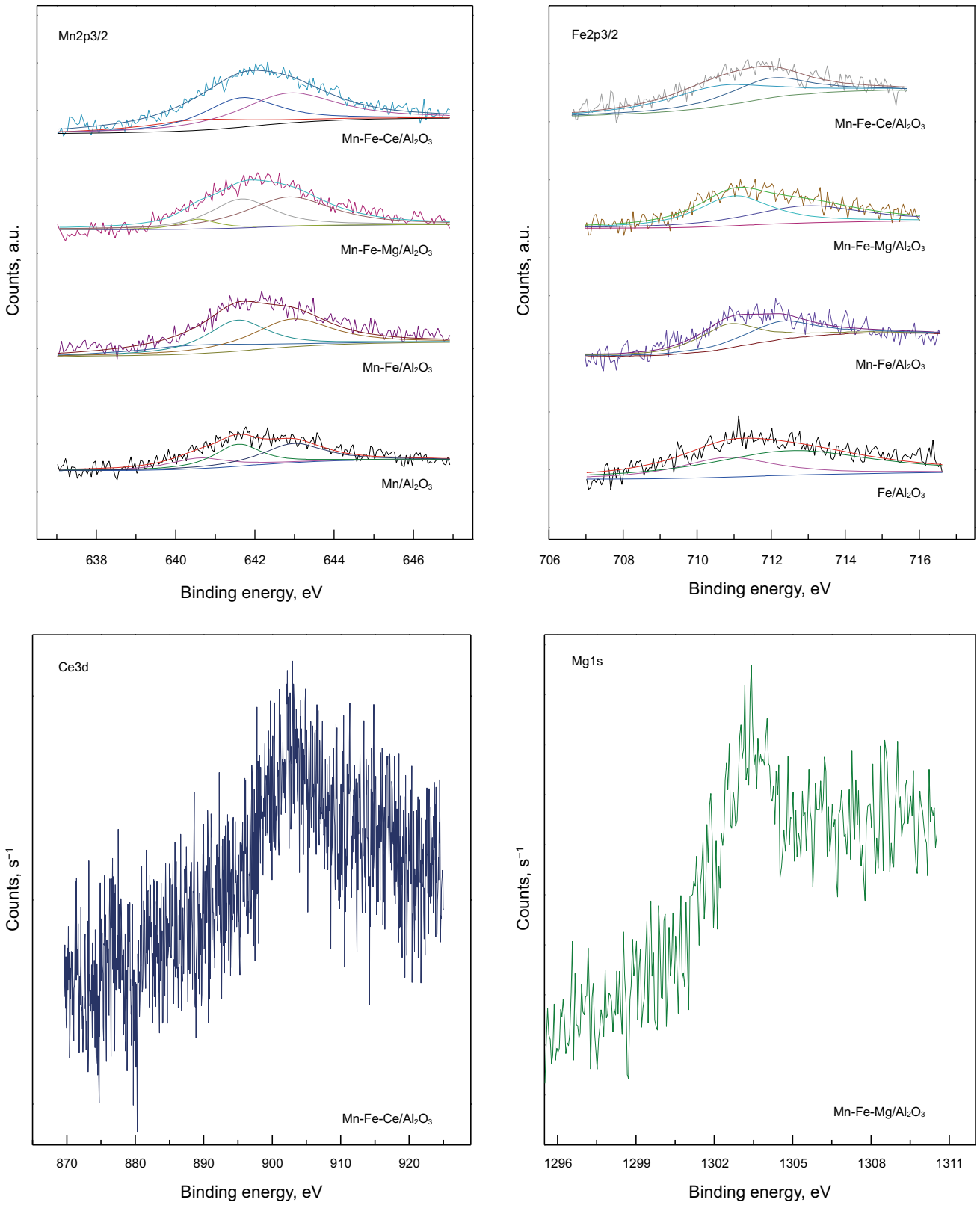

Fig. 6 XPS spectra of Mn2p, Fe2p, Ce3d, and Mg1s of metal oxide-loaded catalysts

Table 2 Binding energies and surface atomic ratios of Mn, Fe, Mg, and Ce elements on catalysts

Items	Fe/Al_2O_3	Mn/Al_2O_3	$Mn–Fe/Al_2O_3$	$Mn–Fe–Mg/Al_2O_3$	$Mn–Fe–Ce/Al_2O_3$
Binding energies					
Mn2p	–	641.8	642.2	642.2	642.2
Fe2p	711.1	–	711.9	711.5	711.7
Ce3d	–	–	–	–	903.0
Mg1s	–	–	–	1303.2	
Metal oxides value state					
Mn^{2+}:Mn^{3+}:Mn^{4+}	–	0.22:0.37:0.41	0.22:0.36:0.42	0.10:0.38:0.53	012:0.39:0.51
Fe^{2+}:Fe^{3+}	0.31:0.69	–	0.52:0.48	0.50:0.50	0.57:0.43
Surface atomic ratio					
Mn2p/Al2p	–	0.015	0.016	0.014	0.015
Fe2p/Al2p	0.016	–	0.018	0.011	0.013
Mg1s/Al2p	–	–	–	0.010	
Ce3d/Al2p	–	–	–		0.004
(Mn2p + Fe2p + Mg1s + Ce3d)/Al2p	0.016	0.015	0.034	0.035	0.032

gas collector. An aliquot of 100 mL of PRW-ROC and 0.5 g of catalyst were added in the reactor at 30 °C. The gaseous ozone was then introduced through a porous diffuser at the bottom of the reactor with a flow rate of 5 mg/min. The experiments were carried out under varying the initial pH values (adjusted with 1 N NaOH or HCl) and reaction times. After treatment, dried oxygen was blown into the PRW-ROC at a rate of 3.0 L/min to quench the reaction and eliminate the residual ozone. The resulting suspension was filtered (Whatman Qualitative No. 5) to separate catalyst particles prior to further analysis at various intervals. The ·OH quenching experiments were performed to determine the oxidation mechanism. The ·OH scavengers, *tert*-butanol (*t*BA), and sodium bicarbonate ($NaHCO_3$) were added into PRW-ROC (0.5 and 1.0 g/L, respectively) prior to experiments. All the experiments were performed in triplicate.

The pH and conductivity were measured with a MP 220 pH meter (Mettler Toledo, Switzerland) and a CD400 conductivity meter (Alalis, China), respectively. The leaching of Ce and Mg elements was measured with an AAnalyst atomic absorption spectrometer (PerkinElmer, USA) using a nitrous oxide/oxygen–acetylene flame. The BOD_5 was tested on a BODTrak II BOD meter (HACH, USA). The COD was measured with a CTL-12 COD meter (HATO, China). The COD removal was calculated using the following equation:

$$\text{COD removal} = \left([\text{COD}]_0 - [\text{COD}]_1\right)/[\text{COD}]_0 \quad (1)$$

3 Results and discussion

3.1 Catalytic performances of catalysts

The COD removal from PRW-ROC using COPs increased using Al_2O_3 and metal oxide-loaded Al_2O_3. Ozonation catalyzed using $Mn–Fe–Mg/Al_2O_3$ ($Mn–Fe–Mg/Al_2O_3$-COP) resulted in an increased COD removal (57.3%) compared with the other catalysts, $Mn–Fe-Ce/Al_2O_3$-COP (56.6%), $Mn–Fe/Al_2O_3$-COP (55.8%), Fe/Al_2O_3-COP (52.0%), Fe/Al_2O_3 (s)-COP (53.8%), Mn/Al_2O_3-COP (51.3%), Mn/Al_2O_3 (s)-COP (53.5%), and Al_2O_3-COP (45.2%). It was especially significant when compared with single oxide ozonation (33.4%) using a 40-min treatment (Fig. 1). The surface content of loaded Fe_2O_3 or MnO was about 4.3 wt% for Fe/Al_2O_3 (s) and Mn/Al_2O_3 (s), almost double compared with Fe/Al_2O_3 and Mn/Al_2O_3 (2.1 wt%). The increased Fe and Mn oxide contents resulted only in a limited performance improvement for COD removal. In comparison, composite metal oxide-loaded Al_2O_3 was more effective at equivalent loadings (about 4.2 wt%), suggesting synergistic effects. For $Mn–Fe–Mg/Al_2O_3$, $Mn–Fe–Ce/Al_2O_3$, $Mn–Fe/Al_2O_3$, Fe/Al_2O_3, and Mn/Al_2O_3 composites, the content of Fe_2O_3 and MnO was 2.1 wt%, and MgO and CeO_2 were above 0.3 wt% based on XRF analysis. Further investigation focused on utilization of $Mn–Fe–Ce/Al_2O_3$, $Mn–Fe–Mg/Al_2O_3$, $Mn–Fe/Al_2O_3$, Mn/Al_2O_3, Fe/Al_2O_3, and Al_2O_3 catalysts.

3.2 Characteristics of catalysts

The metal oxide-loaded Al_2O_3 showed typical γ-Al_2O_3 diffraction peaks (Fig. 2). Obvious XRD diffraction peaks from the metal oxides were not observed, due to the low loading or amorphous status. Using TEM, it was determined that the deposited metal oxides formed micro-agglomerates in irregular shapes and sizes on the surface of Al_2O_3 (Fig. 3), and that based on SEM, the surface morphology of Al_2O_3 itself was little changed.

Adsorption–desorption isotherms and pore distributions varied among Al_2O_3 and metal oxide-loaded Al_2O_3 catalysts (Fig. 4a, b). According to IUPAC classification, the isotherms of these catalysts suggest a typical type IV mesopore structure (Xu and Pang 2004). A hysteresis loop attributed to type H_1 was observed for Al_2O_3, Fe/Al_2O_3, Mn/Al_2O_3, $Fe–Mn/Al_2O_3$, and $Mn–Fe–Ce/Al_2O_3$, suggesting uniform shape and pore size. The hysteresis loop determined for $Mn–Fe–Mg/Al_2O_3$, however, resulted in a combination of H_1 and H_3 types. This suggests the potential presence of silt pores that are a result of metal oxide particle accumulation. Different hysteresis types are potentially a result of interactions between the oxides and the Al_2O_3 support. All deposited oxide catalysts have a pronounced pore distribution peak at 5–6 nm. The surface areas (S_{BET}), pore volumes (V_P), and average pore sizes (D_a) were 230–250 m^2/g, 0.35–0.38 cm^3/g, and 5.7–6.1 nm, respectively (Table 1). $Mn–Fe–Mg/Al_2O_3$ showed the lowest S_{BET} and V_P values among these catalysts.

Figure 5 shows the UV–Vis spectra of metal oxide-loaded catalysts. Fe/Al_2O_3 had a wide absorbance peak with a lower intensity centered at 200–600 nm, attributed to isolated Fe^{3+}, oligomeric FeO_x clusters, and large Fe_2O_3 particles (Santhosh Kumar et al. 2004). Mn/Al_2O_3 displayed an absorption peak centered at 250 nm and a wide peak with lower intensity centered at 400–600 nm, associated with a charge transfer (CT) $O^{2-} \rightarrow Mn^{2+}$ and poorly resolved absorbance bands (d-d transitions) from Mn^{3+}- and Mn^{4+}-oxo species, respectively (Wu et al. 2015). $Mn–Fe/Al_2O_3$ exhibited peaks at 250, 350, and 480 nm, due to composite Fe and/or Mn oxide presence. $Mn–Fe–Mg/Al_2O_3$ and $Mn–Fe–Ce/Al_2O_3$ showed significantly increased absorbance intensity at 250 nm, suggesting homogenous dispersion of Ce and Mg oxides.

Figure 6 shows the XPS spectra of Mn2p, Fe2p, Mg1s, and Ce3d for metal oxide-loaded catalysts. Table 2 shows the binding energies and surface atomic ratios for these metallic elements. The Mn2p3/2 peaks of Mn/Al_2O_3, $Mn–Fe/Al_2O_3$, $Mn–Fe–Mg/Al_2O_3$, and $Mn–Fe–Mg/Al_2O_3$ are attributed to Mn^{2+} oxides (MnO or $Mn(OH)_2$), Mn^{3+} oxides (Mn_2O_3 or MnOOH), and Mn^{4+} oxide (MnO_2) (Zhang et al. 2015). The Fe2p3/2 peaks of Fe/Al_2O_3, $Mn–Fe/Al_2O_3$, $Mn–Fe–Mg/Al_2O_3$, and $Mn–Fe–Mg/Al_2O_3$ are related to Fe^{2+} oxides (FeO or $Fe(OH)_2$) and Fe^{3+} oxides (Fe_2O_3 or FeOOH) (Shwana et al. 2015). The surface atomic ratios of Fe2p to Al2p (0.011 ~ 0.018) and Mn2p to Al2p (0.014 ~ 0.016) for catalysts changed little and were close to the bulk molar ratio of Fe to Al (0.0129) and Mn to Al (0.01547). The asymmetrical distribution of the Mg1s peak is likely a result of interactions between Mg, Mn, and Fe. The surface atomic ratio (0.010) of Mg1s to

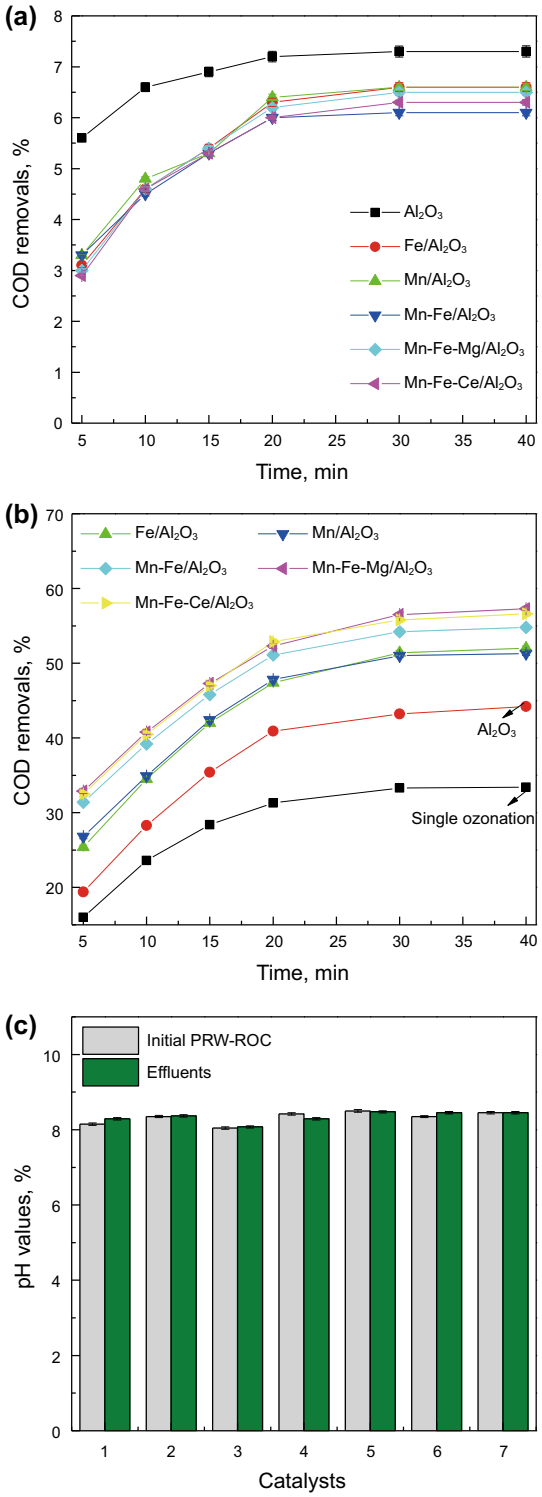

Fig. 7 COD removal from PRW-ROC by adsorption (**a**) and over single ozonation and various COPs (**b**); pH value changes of PRW-ROC over single ozonation and various COPs (**c**): *1* single ozonation, *2* Al_2O_3-COP, *3* Fe/Al_2O_3-COP, *4* Mn/Al_2O_3-COP, *5* $Mn–Fe/Al_2O_3$-COP, *6* $Mn–Fe–Mg/Al_2O_3$-COP, and *7* $Mn–Fe–Ce/Al_2O_3$-COP

Table 3 Influences of ·OH scavengers on COD removals of PRW-ROC using Mn–Fe/Al_2O_3-COP, Mn–Fe–Mg/Al_2O_3-COP, and Mn–Fe–Ce/Al_2O_3-COP

Systems	COD removals (%)				
	No ·OH scavenger	*t*BA		$NaHCO_3$	
		0.5, g/L	1.0, g/L	0.5, g/L	1.0, g/L
Mn–Fe/Al_2O_3-COP	55.8	24.9	22.7	30.5	28.7
Mn–Fe–Mg/Al_2O_3-COP	57.3	37.6	14.9	34.3	31.3
Mn–Fe–Ce/Al_2O_3-COP	56.6	34.9	16.9	31.7	27.8

0.5 g catalyst, 5 mg/min ozone, 30 °C, and 40 min

Al2p for Mn–Fe–Mg/Al_2O_3 is far greater than that in bulk (0.0038), suggesting high surface area distribution of the Mg oxide. Similarly the surface atomic ratio (0.004) of Ce3d to Al2p for Mn–Fe–Ce/Al_2O_3 is higher than that in bulk (0.0009), again suggesting high surface area dispersion of Ce^{4+} oxide (Ding et al. 2016). The surface atomic ratios of the sum of Mn2p + Fe2p + Mg1s + Ce3d to Al2p for Mn–Fe–Mg/Al_2O_3, Mn–Fe–Ce/Al_2O_3, and Mn–Fe/Al_2O_3 catalysts were similar to each other and doubled compared to Mn/Al_2O_3 and Fe/Al_2O_3.

3.3 Mechanisms of catalytic ozonation

The adsorption onto the catalysts reached saturation by 40 min. Adsorption on Al_2O_3, Fe/Al_2O_3, Mn/Al_2O_3, Mn–Fe/Al_2O_3, Mn–Fe–Mg/Al_2O_3, and Mn–Fe–Ce/Al_2O_3 contributed to COD removals by 7.3%, 6.6%, 6.6%, 6.1%, 6.5%, and 6.3%, respectively (Fig. 7a). No significant differences for adsorption capacity among catalysts were observed, likely due to similar surface areas (Table 1). COD removals using various COPs increased by 23.9%–11.8% compared with single ozonation (Fig. 7b). These results are significantly greater than simple adsorption (7.3%–6.1%). The observed difference can be attributed to the application of catalytic ozonation. Mn–Fe/Al_2O_3 exhibited better catalytic performance than Mn/Al_2O_3 and Fe/Al_2O_3, and the introduction of Mg and/or Ce further improved the catalytic performance. The active surface areas for all the material comparisons were similar and would not have an impact on differences in catalytic activity (Table 1). The enhanced catalytic activity of Mn–Fe–Mg/Al_2O_3, Mn–Fe–Ce/Al_2O_3, and Mn–Fe/Al_2O_3 resulted from the metal oxide components themselves, interactions between the metal oxides, interactions between the metal oxides and Al_2O_3 support, as well as its environment (Table 2). Similar relationships between reaction times and COD removals using different COPs were obtained (Fig. 7b), suggesting the similarity of catalytic mechanisms for the various catalysts. Small pH changes in the effluents from single ozonation and COPs were found compared to that of the initial PRW-ROC (Fig. 7c).

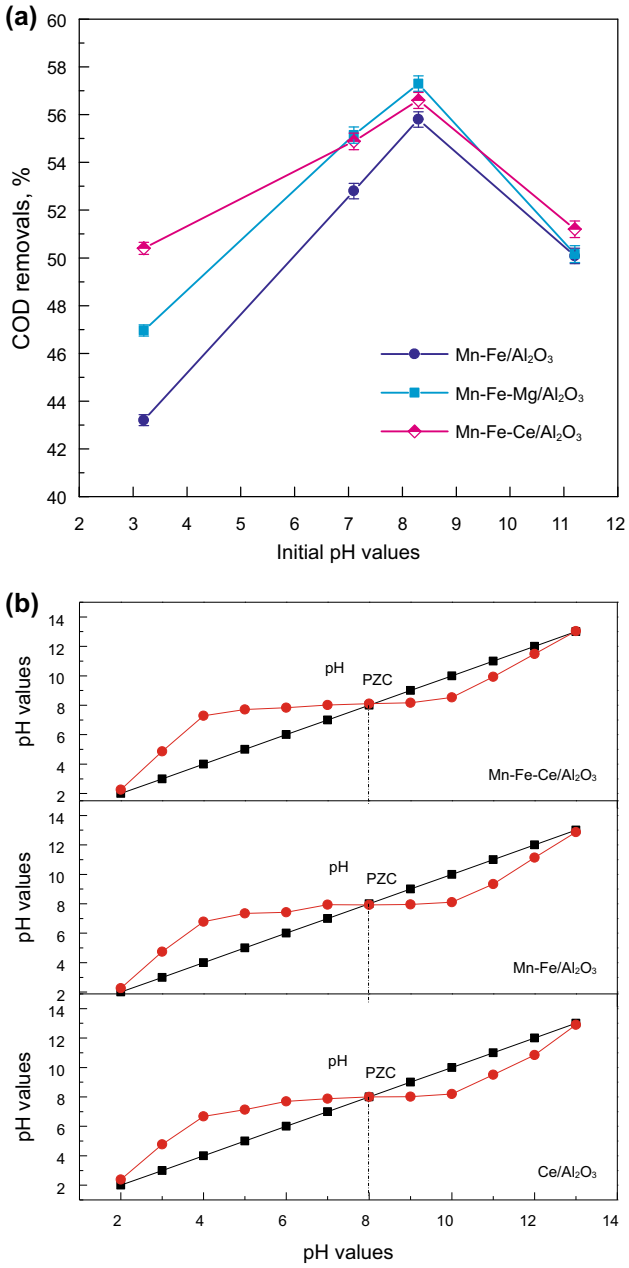

Fig. 8 **a** Influences of the initial pH values on COD removals using Mn–Fe/Al_2O_3-COP, Mn–Fe–Mg/Al_2O_3-COP, and Mn–Fe–Ce/Al_2O_3-COP; and **b** pH_{pzc} values of three catalysts

Several reports have suggested that ·OH generation induced by catalysts increased removal of pollutants during COP treatment (Qi et al. 2013). In order to identify whether these treatments result in the generation of ·OH, COD removals in the presence of *t*BA and $NaHCO_3$ were examined. From this it was determined that the COD removal of PRW-ROC was lessened due to the introduction of *t*BA and $NaHCO_3$ in bulk (Table 3). $NaHCO_3$ may impair catalytic decomposition of ozone into ·OH on the catalyst surface because of its high affinity to Lewis acid sites on the catalyst surface. In contrast, *t*BA can quench aqueous ozone decomposition by reacting with ·OH in bulk, generating inert intermediates. As such, the catalytic ozonation of PRW-ROC was dominated by ·OH both on the catalyst surface and in bulk in COPs over Mn–Fe–Mg/Al_2O_3, Mn–Fe–Ce/Al_2O_3, and Mn–Fe/Al_2O_3. The decreased extent of COD removals by both *t*BA and $NaHCO_3$ in Mn–Fe–Mg/Al_2O_3-COP and Mn–Fe–Ce/Al_2O_3-COP was greater than that in Mn–Fe/Al_2O_3-COP. It is reasonable to then expect that the introduction of small concentrations of Mg or Ce can be used to further promote ·OH generation. In addition, the inhibitory effect for ·OH generation using *t*BA was greater than that by $NaHCO_3$, suggesting more ·OH oxidation occurred in bulk rather than on the catalyst surface. COD was still, however, reduced in spite of the addition of ·OH scavengers and can be ascribed to direct ozonation.

Initial pH values that were either acidic, at the pH_{pzc}, or alkaline, significantly influenced the COD removal during COP treatment of PRW-ROC (Fig. 8a). An initial pH value of 3 resulted in reduced efficiency of COP and was probably a result of the metal species being leached from the catalyst. Initial pH values of 8.3 (Fig. 8a) were close to the pH_{pzc} (Fig. 8b) of the three composite catalysts and resulted in efficient COD removal. Alkaline pH values around 11 may result in the formation of carbonate and bicarbonate during organic mineralization, again decreasing the efficiency of COP (Xiong et al. 2003). The positive impact of surface hydroxyl groups (–OH), on active surfaces, has been determined for the removal of organics (Lu et al. 2014; Zhang et al. 2007, 2008). It is believed that pH values near the pH_{pzc} of the catalyst can result in accelerated ·OH generation, due to a neutral –OH state (Qi et al. 2012). Based on ·OH quenching experiments and the impact of initial pH values, the surface –OH likely does have a significant role in COP treatment of PRW-ROC. The surface MnOOH and FeOOH of catalysts are the principle drivers for COP according to XPS results (Table 2). The enhanced COD removal compared with Mn–Fe–Mg/Al_2O_3 and Mn–Fe–Ce/Al_2O_3 may suggest greater ·OH-related activity due to interactions between the various metal oxides and/or changes of metallic states influenced by the environment. Ozone reacts with surface –OH groups during COP treatment and results in highly active ·OH generation in bulk and/or on the surface, resulting in organics oxidation (Fig. 9).

3.4 Reusability and stability of catalysts

Catalysts were reused ten times for COD removal from PRW-ROC with Al_2O_3-COP, Mn–Fe–Mg/Al_2O_3-COP, and Mn–Fe–Ce/Al_2O_3-COP. Conditions for experiments included, 0.5 g catalyst, 5 mg/min ozone, 30 °C, 40 min treatment, and initial pH values. COD removal from PRW-

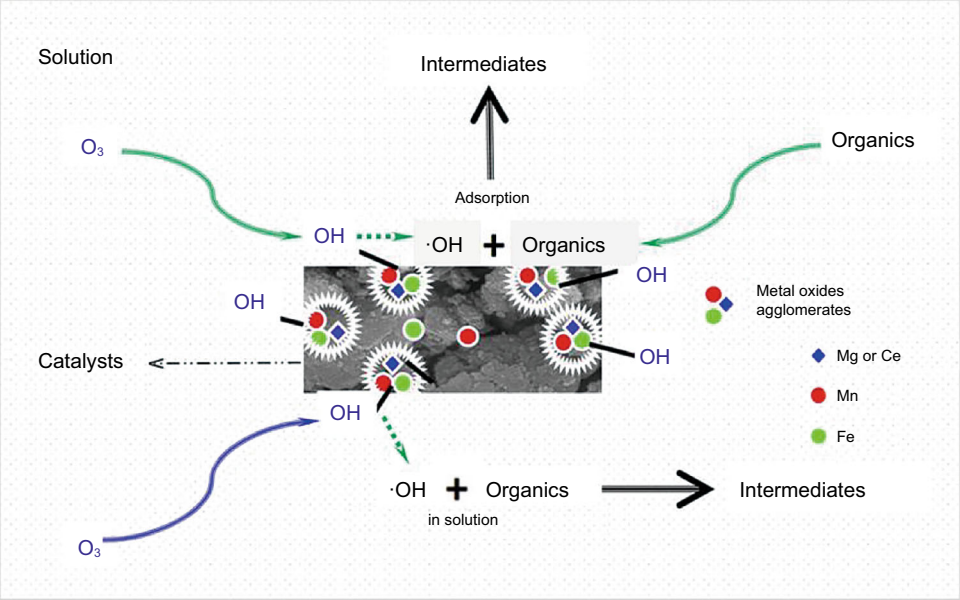

Fig. 9 Proposed ozonation mechanisms of organics in PRW-ROC upon Mn–Fe–Mg/Al_2O_3 and Mn–Fe–Ce/Al_2O_3

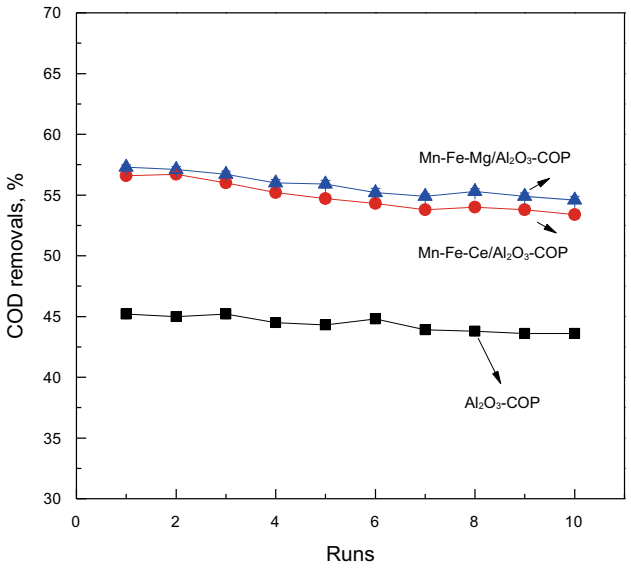

Fig. 10 COD removals in 10 COP runs using Al_2O_3, Mn–Fe–Mg/Al_2O_3, and Mn–Fe–Ce/Al_2O_3

ROC was maintained within the range of 57.3%–54.6% for Mn–Fe–Mg/Al_2O_3-COP and 55.6%–53.4% for Mn–Fe–Ce/Al_2O_3-COP, far greater than Al_2O_3-COP (45.2%–43.6%) (Fig. 10). Single ozonation and adsorption had relatively low efficiency for the removal of bio-recalcitrant organics from PRW-ROC. By using Mn–Fe–Mg/Al_2O_3-COP and Mn–Fe-Ce/Al_2O_3-COP, bio-recalcitrant organics in PRW-ROC were degraded by the greater generation of ·OH compared with single ozonation (Table 3). The PRW-ROC was successfully treated by utilizing the composite metal oxide-loaded Al_2O_3 during catalyzed ozonation to reduce the COD value to below 60 mg/L. This value met the Emission Standard of Pollutants for Petroleum Refining Industry of China (GB 31570-2015). No significant leaching of Ce or Mg elements was detected in Mn–Fe–Ce/Al_2O_3-COP or Mn–Fe–Mg/Al_2O_3-COP. These results showed that Mn–Fe–Mg/Al_2O_3 and Mn–Fe–Ce/Al_2O_3 catalysts were stable and reuseable and could increase the efficiency of ozonation treatments of PRW-ROC.

4 Conclusions

The composite metal oxide-loaded Al_2O_3 catalysts, Mn–Fe–Mg/Al_2O_3 and Mn–Fe–Ce/Al_2O_3, were prepared and used for efficient ozonation of PRW-ROC. The 100–300 nm multivalent metal oxides of Mn (Mn^{2+}, Mn^{3+} and Mn^{4+}), Fe (Fe^{2+} and Fe^{3+}), and Mg (Mg^{2+})/Ce (Ce^{4+}) were highly dispersed on the Al_2O_3 support. COD removals by Mn–Fe–Mg/Al_2O_3-COP and Mn–Fe–Ce/Al_2O_3-COP increased by 23.9% and 23.2%, respectively, relative to single ozonation. Mn–Fe–Mg/Al_2O_3 and Mn–Fe–Ce/Al_2O_3 promote ·OH generation and ·OH-mediated oxidation and are effective at degrading bio-recalcitrant organics in PRW-ROC. The composite metal oxide-loaded Al_2O_3-catalyzed ozonation exhibited great potential and industrial feasibility for advanced treatment of bio-recalcitrant PRW-ROC.

Acknowledgements This project was supported in part by the National Science and Technology Major Project of China (No. 2016ZX05040-003).

References

Altenor S, Carene B, Emmanuel E, et al. Adsorption studies of methylene blue and phenol onto vetiver roots activated carbon prepared by chemical activation. J Hazard Mater. 2009;165:1029–39. doi:10.1016/j.jhazmat.2008.10.133.

Bagastyo AY, Keller J, Poussade Y, et al. Characterization and removal of recalcitrants in reverse osmosis concentrates from water reclamation plants. Water Res. 2013;45:2415–27. doi:10.1016/j.watres.2011.01.024.

Bagastyo AY, Radjenovic J, Mu Y, et al. Electrochemical oxidation of reverse osmosis concentrate on mixed metal oxide (MMO) titanium coated electrode. Water Res. 2011;45:4951–9. doi:10.1016/j.watres.2011.01.024.

Bing J, Hu C, Zhang L. Enhanced mineralization of pharmaceuticals by surface oxidation over mesoporous γ-Ti–Al_2O_3 suspension with ozone. Appl Catal B Environ. 2017;202:118–26. doi:10.1016/j.apcatb.2016.09.019.

Bing J, Wang X, Lan B, et al. Characterization and reactivity of cerium loaded MCM-41 for p-chlorobenzoic acid mineralization with ozone. Sep Purif Technol. 2013;118:479–86. doi:10.1016/j.seppur.2013.07.048.

Chen C, Yoza BA, Wang Y, et al. Catalytic ozonation of petroleum refinery wastewater utilizing Mn–Fe–Cu/Al_2O_3 catalyst. Environ Sci Pollut Res. 2015;22(7):5552–62. doi:10.1007/s11356-015-4136-0.

Chen X, Zhang Z, Liu L, et al. RO applications in China: history, current status, and driving forces. Desalination. 2016;397:185–93. doi:10.1016/j.desal.2016.07.001.

Dialynas E, Mantzavinos D, Diamadopoulos E. Advanced treatment of the reverse osmosis concentrate produced during reclamation of municipal wastewater. Water Res. 2008;42:4603–8. doi:10.1016/j.watres.2008.08.008.

Ding J, Lin J, Xiao J, ZhangY Zhong Q, Zhang S, Guo L, Fan M. Effect of fluoride doping for catalytic ozonation of low-temperature denitrification over cerium-titanium catalyst. J Alloy Compd. 2016;665:411–7. doi:10.1016/j.jallcom.2016.01.040.

Einaga H, Futamura S. Oxidation behavior of cyclohexane on alumina-supported manganese oxides with ozone. Appl Catal B: Environ. 2005;60:49–55. doi:10.1016/j.apcatb.2005.02.017.

Joo SH, Tansel B. Novel technologies for reverse osmosis concentrate treatment: a review. J Environ Manag. 2015;150:322–35. doi:10.1016/j.jenvman.2014.10.027.

Keykavoos R, Mankidy R, Ma H, et al. Mineralization of bisphenol A by catalytic ozonation over alumina. Sep Purif Technol. 2013;107:310–7. doi:10.1016/j.seppur.2013.01.050.

Lu X, Huang X, Ma J. Removal of trace mercury (II) from aqueous solution by in situ formed Mn–Fe(hydr) oxides. J Hazard Mater. 2014;280:71–8. doi:10.1016/j.jhazmat.2014.07.056.

Moreira FC, Boaventura RAR, Brillas E, et al. Electrochemical advanced oxidation processes: a review on their application to synthetic and real wastewaters. Appl Catal B Environ. 2017;202:217–61. doi:10.1016/j.apcatb.2016.08.037.

Moussavi G, Aghapour AA, Yaghmaeian K. The degradation and mineralization of catechol using ozonation catalyzed with MgO/GAC composite in a fluidized bed reactor. Chem Eng J. 2014;249:302–10. doi:10.1016/j.cej.2014.03.059.

Moussavi G, Mahmoudi M. Degradation and biodegradability improvement of the reactive red 198 azo dye using catalytic ozonation with MgO nanocrystals. Chem Eng J. 2009;152:1–7. doi:10.1016/j.cej.2009.03.014.

Nie Y, Hu C, Li N, et al. Inhibition of bromate formation by surface reduction in catalytic ozonation of organic pollutants over β-FeOOH/Al_2O_3. Appl Catal B Environ. 2014;147:287–92. doi:10.1016/j.apcatb.2013.09.005.

Pocostales P, Álvarez P, Beltrán FJ. Catalytic ozonation promoted by alumina-based catalysts for the removal of some pharmaceutical compounds from water. Chem Eng J. 2011;168:1289–95. doi:10.1016/j.watres.2011.10.046.

Pérez-González A, Urtiaga AM, Ibáñez R, et al. State of the art and review on the treatment technologies of water reverse osmosis concentrates. Water Res. 2012;46:267–83. doi:10.1016/j.watres.2011.10.046.

Qi F, Xu B, Chen Z, et al. Catalytic ozonation of 2-isopropyl-3-methoxypyrazine in water by γ-AlOOH and γ-Al_2O_3: comparison of removal efficiency and mechanism. Chem Eng J. 2013;219:527–36. doi:10.1016/j.apcatb.2012.04.003.

Qi F, Xu B, Chen Z, et al. Influence of aluminum oxides surface properties on catalyzed ozonation of 2,4,6-trichloroanisole. Sep Purif Technol. 2009;2:405–10.

Qi F, Xu B, Zhao L, et al. Comparison of the efficiency and mechanism of catalytic ozonation of 2, 4, 6-trichloroanisole by iron and manganese modified bauxite. Appl Catal B Environ. 2012;121–122:171–81. doi:10.1016/j.apcatb.2012.04.003.

Ren Y, Yuan Y, Lai B, et al. Treatment of reverse osmosis (RO) concentrate by the combined Fe/Cu/air and Fenton process (1stFe/Cu/air-Fenton-2ndFe/Cu/air). J Hazard Mater. 2016;302:36–44. doi:10.1016/j.jhazmat.2015.09.025.

Rezaei F, Moussavi G, Bakhtiari AR, Yamini Y. Toluene removal from waste air stream by the catalytic ozonation process with MgO/GAC composite as catalyst. J Hazard Mater. 2016;306-8. doi:10.1016/j.jhazmat.2015.11.026.

Rosal R, Gonzalo MS, Rodríguez A, et al. Catalytic ozonation of fenofibric acid over alumina-supported manganese oxide. J Hazard Mater. 2010a;183:271–8. doi:10.1016/j.jhazmat.2010.07.021.

Rosal R, Gonzalo MS, Rodríguez A, et al. Catalytic ozonation of atrazine and linuron on MnO_x/Al_2O_3 and MnO_x/SBA-15 in a fixed bed reactor. Chem Eng J. 2010b;165:806–12.

Santhosh Kumar M, Schwidder M, Grünert W, Brückner A. On the nature of different iron sites and their catalytic role in Fe-ZSM-5 DeNO*x* catalysts: new insights by a combined EPR and UV/VIS spectroscopic approach. J Catal. 2004;227:384–97. doi:10.1016/j.jcat.2004.08.003.

Santiago-Morales J, Gómez MJ, Herrera S, et al. Oxidative and photochemical processes for the removal of galaxolide and tonalide from wastewater. Water Res. 2012;46:4435–47. doi:10.1016/j.watres.2012.05.051.

Shwana S, Jansson J, Olsson L, et al. Chemical deactivation of H-BEA and Fe-BEA as NH_3-SCR catalysts—effect of potassium. Appl Catal B Environ. 2015;166–167:277–86. doi:10.1016/S1001-0742(09)60298-9.

Tong S, Shi R, Zhang H, et al. Catalytic performance of Fe_3O_4-CoO/Al_2O_3 catalyst in ozonation of 2-(2,4-dichlorophenoxy)propionic acid, nitrobenzene and oxalic acid in water. J Environ Sci China. 2010;22:1623–8. doi:10.1016/S1001-0742(09)60298-9.

Umar M, Roddick F, Fan L. Impact of coagulation as a pre-treatment for UVC/H_2O_2-biological activated carbon treatment of a municipal wastewater reverse osmosis concentrate. Water Res. 2016;88:12–9. doi:10.1016/j.watres.2015.09.047.

Van Hege K, Verhaege M, Verstraete W. Indirect electrochemical oxidation of reverse osmosis membrane concentrates at boron-doped diamond electrodes. Electrochem Commun. 2002;4:296–300. doi:10.1016/S1388-2481(02)00276-X.

Vittenet J, Aboussaoud W, Mendret J, et al. Catalytic ozonation with γ-Al_2O_3 to enhance the degradation of refractory organics in water. Appl Catal A Gen. 2015;504:519–32. doi:10.1016/j.apcata.2014.10.037.

Wu G, Gao Y, Ma F, et al. Catalytic oxidation of benzyl alcohol over manganese oxide supported on MCM-41 zeolite. Chem Eng J. 2015;271:14–22. doi:10.1016/j.cej.2015.01.119.

Xiong Y, He C, Karlsson HT, et al. Performance of three-phase three-dimensional electrode reactor for the reduction of COD in simulated wastewater-containing phenol. Chemosphere. 2003;50:131–6. doi:10.1016/S0045-6535(02)00609-4.

Xu B, Qi F, De Sun, et al. Cerium doped red mud catalytic ozonation for bezafibrate degradation in wastewater: efficiency, intermediates, and toxicity. Chemosphere. 2016;146:22–31. doi:10.1016/j.chemosphere.2015.12.016.

Xu RR, Pang WQ. Chemistry of zeolites and porous materials. In: Structural analysis and properties of porous materials characterization. Li XP, editor. Beijing: Science Press; 2004. p. 145–9 (**in Chinese**).

Yan H, Lu P, Pan Z, et al. Ce/SBA-15 as a heterogeneous ozonation catalyst for efficient mineralization of dimethyl phthalate. J Mol Catal A Chem. 2013;377:57–64. doi:10.1016/j.molcata.2013.04.032.

Zhang ZF, Liu BS, Wang F, et al. High-temperature desulfurization of hot coal gas on Mo modified Mn/KIT-1 sorbents. Chem Eng J. 2015;272:69–78. doi:10.1016/j.cej.2015.02.091.

Zhang G, Qu H, Liu R, et al. Preparation and evaluation of a novel Fe-Mn binary oxide adsorbent for effective arsenite removal. Water Res. 2007;41:1921–8. doi:10.1016/j.watres.2007.02.009.

Zhang L, Ma J, Yu M. The microtopography of manganese dioxide formed in situ and its adsorptive properties for organic micropollutants. Solid State Sci. 2008;10:148–53. doi:10.1016/j.solidstatesciences.2007.08.013.

Zhou M, Tan Q, Wang Q, et al. Degradation of organics in reverse osmosis concentrate by electro-Fenton process. J Hazard Mater. 2012;215–216:287–93. doi:10.1016/j.jhazmat.2012.02.070.

Zhou Y, Zhu W, Liu F, et al. Catalytic activity of Ru/Al_2O_3 for ozonation of dimethyl phthalate in aqueous solution. Chemosphere. 2007;66:145–50. doi:10.1016/j.chemosphere.2006.04.087.